Published in final edited form as:
Faraday Discuss. 2013 ; 161: 383–459.

Elastic Properties of Polyunsaturated Phosphatidylethanolamines Influence Rhodopsin Function

Walter E. Teague Jr.[a], **Olivier Soubias**[a], **Horia Petrache**[b], **Nola Fuller**[c], **Kirk G. Hines**[a], **R. Peter Rand**[c], and **Klaus Gawrisch**[a]

Horia Petrache: hpetrach@iupui.edu; R. Peter Rand: rrand@brocku.ca; Klaus Gawrisch: gawrisch@helix.nih.gov

[a]Laboratory of Membrane Biochemistry and Biophysics, NIAAA, NIH, Bethesda, MD 20892, USA. Fax: +1-301-594-0035; Tel: +1-301-594-3750

[b]Department of Physics, Indiana Univ.- Perdue Univ., Indianapolis, IN 46202, USA. Fax: +1-317-274-2392; Tel: +1-317-278-6521

[c]Dept. Biol. Sci., Brock Univ., St. Catharines, Ont. L2S 3A1, Canada. Phone:+1-905-688-5550 ext.3388

Abstract

Membranes with a high content of polyunsaturated phosphatidylethanolamines (PE) facilitate formation of metarhodopsin-II (M_{II}), the photointermediate of bovine rhodopsin that activates the G protein transducin. We determined whether M_{II}-formation is quantitatively linked to the elastic properties of PEs. Curvature elasticity of monolayers of the polyunsaturated lipids 18:0–22:$6_{n\text{-}3}$PE, 18:0-22:$5_{n\text{-}6}$PE and the model lipid 18:$1_{n\text{-}9}$-18:$1_{n\text{-}9}$PE were investigated in the inverse hexagonal phase. All three lipids form lipid monolayers with rather low spontaneous radii of curvature of 26–28 Å. In membranes, all three PEs generate high negative curvature elastic stress that shifts the equilibrium of M_I/M_{II} photointermediates of rhodopsin towards M_{II} formation.

Introduction

Phosphoethanolamines (PE) comprise about 40% of retinal and synaptosomal membranes and, within these membranes, about 50% of hydrocarbon chains in PE are the six-fold unsaturated docosahexaenoic acid (22:$6_{n\text{-}}$3, DHA)[1, 2]. It was reported earlier that increased levels of PE significantly boost formation of the photointermediate metarhodopsin-II (M_{II}) that is capable of activating the G protein transducin[3, 4]. PE lipids have the tendency to form inverse hexagonal lipid phases (H_{II}) composed of highly curved monolayers with small area per lipid at the PE headgroup and a larger area near the terminal methyl groups of hydrocarbon chains. When forced into a lamellar arrangement, those monolayers are under considerable negative curvature elastic stress.

Here we investigated the influence of hydrocarbon chain polyunsaturation on coefficients of monolayer curvature elasticity for the polyunsaturated lipids 18:0-22:$6_{n\text{-}3}$PE and 18:0-22:$5_{n\text{-}6}$PE and compared them to the model lipid 18:$1_{n\text{-}9}$-18:$1_{n\text{-}9}$PE (DOPE). Using a combination of ^{31}P NMR, ^{2}H NMR, magic angle spinning (MAS) ^{1}H-NMR, and x-ray diffractometry, we determined the phase state of the lipid water dispersions, the order parameters of lipid hydrocarbon chains, the water content of inverse hexagonal phases, and the repeat spacing of inverse cylindrical micelles in the H_{II} phase, respectively. The energetics of bending lipid monolayers were followed by dehydrating the H_{II} phase under

Correspondence to: Klaus Gawrisch, gawrisch@helix.nih.gov.

controlled osmotic pressure induced by polyethylene glycol (PEG)/water solutions[5]. The bending elastic modulus, K_{cp}, the spontaneous radius of monolayer curvature, R_{op}, and the area per lipid molecule at the pivotal plane, $A_{p,}$ where area per lipid remains constant upon monolayer bending, were determined by fitting the experimental data to a model developed earlier by Rand, Gruner, and Parsegian[6, 7].

Bovine rhodopsin was reconstituted into proteoliposomes composed of the PEs at concentrations from 0–75 mol% in 16:0-18:$1_{n\text{-}9}$PC (POPC). After a flash of light, the equilibrium of the photointermediates metarhodopsin-I (M_I) and metarhodopsin-II (M_{II}) was measured spectrophotometrically following procedures developed by the Litman laboratory[8]. The predicted shift in the M_I/M_{II} equilibrium towards M_{II} from negative curvature elastic stress in membranes is compared with experimentally measured M_I/M_{II} equilibria.

Materials and Methods

Sample preparation

The phospholipids were synthesized by Avanti Polar Lipids (Alabaster, AL).

Lipid Samples—Polyunsaturated PEs are particularly prone to oxidation. Therefore all sample handling was conducted in a model 855-AC controlled atmosphere chamber (PLAS LAB, Lansing, MI) filled with oxygen-free argon or nitrogen gas. The antioxidant butylated hydroxytoluene (BHT) was added to the lipids at a molar ratio of 1 BHT per 100 lipids. All solutions were carefully degassed before use. Oxidation of lipids was monitored by recording ^{1}H high-resolution NMR spectra of small aliquots of the samples in deuterated chloroform before and after the experiments. The intensity of resonances of doubled bonds at 5.3 ppm and of the methylene groups between double bonds at 2.8 ppm were compared to intensity of phosphoethanolamine and glycerol resonances. Only data from samples with negligible oxidation (< 1 mol%) were used for data analysis.

For NMR and x-ray experiments, 10-mg samples of PE were dried under a stream of ultra-pure argon or nitrogen in a rapidly rotating 5mm glass tube. The sample was hydrated by the addition of 200 μl of deuterium depleted water and the tube was capped and rotated for 30 minutes and the sample collected at the bottom of the tube by centrifugation. The sample was then removed with a spatula and placed in an 8-mm long section of 4-mm wide dialysis tubing with a molecular weight cut-off of 8,000 (Spectra/Por, Spectrum Labs, Rancho Dominguez, CA). The tubing was closed with clips and equilibrated over a period of two hours in a solution of polyethylene glycol MW=20,000 (PEG20,000, Fluka) in water at 30°C using PEG concentrations of 3, 6, 10, 15, 20, 25, 30, 35, 40, 45, 50, and 55 wt%, respectively. Rapid equilibration of water content in PE samples with the PEG solutions was critical to prevent oxidation (<1%). This was achieved by continuously pumping the PEG solution past the dialysis tubing in a chamber using a Masterflex L/S peristaltic pump (Cole-Parmer, Court Vernon Hills, IL). This procedure eliminates water gradients that tend to form near the surface of the dialysis membrane in the viscous PEG solution and decreases the equilibration time to about one hour. Equilibrated samples were transferred into sealed glass containers for ^{31}P NMR and ^{2}H NMR analysis and into to a 4 mm rotor for magic-angle spinning (MAS) ^{1}H NMR analysis of water content. A duplicate set of samples was prepared for measurement of the dimensions of the H_{II} phase using x-ray diffraction analysis.

Rhodopsin samples—Rhodopsin was purified from bovine retinas using procedures that were developed by the Litman laboratory [9]. Rhodopsin fractions in 3 wt % octylglucoside (OG) which gave a UV-vis absorption intensity ratio at 280 nm/500 nm of 1.8 were used.

The rhodopsin-OG solution was added to lipid-OG mixed micelles for a final OG/lipid molar ratio of 10/1 and a rhodopsin/phospholipid molar ratio of 1/250. Samples were homogenized by vortexing and then equilibrated for 12 h under argon. Subsequently, this rhodopsin/lipid solution was added dropwise at a rate of 400 μL/min to deoxygenated PIPES buffer (10 mM PIPES, 100 mM NaCl, 50 μM DTPA, pH = 7.0) under rapid stirring, resulting in formation of unilamellar proteoliposomes. Typically, the final OG concentration was 7.2 mM, which is well below the critical micelle concentration. The proteoliposome dispersion (2.5–3 mL) was then dialyzed against 1 L of PIPES buffer (Slide-A-Lyzer membrane, 10 kDa cutoff; Pierce, Rockford, IL). The buffer was exchanged three times over 24 h. The final rhodopsin concentration in the samples was measured by light absorption at 500 nm assuming a molar extinction coefficient ε_{500}=40,600 M^{-1} cm^{-1} [10]. The concentration of residual OG in the lipid bilayers was lower than 0.4 mol% of the lipid concentration as determined by high-resolution ^{1}H NMR.

NMR—Solid-state ^{31}P- and ^{2}H NMR spectra were acquired on a DMX300 spectrometer equipped with a ^{1}H-X probe with a solenoid coil (Bruker BioSpin, Billerica, MA). Experiments were conducted at a resonance frequency of 121.47 MHz and a spectral width of 125 kHz using a Hahn-echo, 90°-τ–180°-τ-acquire, pulse sequence and broad-band decoupling of protons. ^{2}H NMR spectra were acquired at a resonance frequency of 46.1 MHz using a quadrupolar echo pulse sequence 90°-τ-90^{90}-τ-acquire. ^{1}H-MAS NMR spectra were acquired on an AV800 spectrometer equipped with a high resolution ^{1}H/^{13}C/^{2}H 4-mm MAS NMR probe (Bruker BioSpin, Billerica, MA) at a resonance frequency of 800.18 MHz and a MAS spinning frequency of 10 kHz.

X-ray diffraction—After equilibration with PEG/water solutions, the PE was filled into cells made of aluminum with mylar windows. Extra PEG solution was also loaded in the cell to maintain lipid hydration. Sample temperature was controlled to 30 ±0.5°C by thermoelectric elements beneath the cell. X-ray diffraction patterns were acquired using an Elliot GX-13 rotating-anode x-ray generator equipped with two x-ray mirrors and a Frank-type camera. Kodak image plates were used for detection. They were scanned and digitized by a Fujifilm BAS-2500 plate reader at 50-μm pixel size resolution. The phase state of lipids was characterized by its lattice dimension. Hexagonal phases gave spacings in the ratios of 1, 1/√3, 1/√4,1 /√7, 1 /√9,1 /√12, etc. which were used to measure the lattice dimension d_{hex}.

Lipid density—The mass density of lipids in the H_{II} phase was determined by centrifugation in H_2O/^2H_2O mixtures. The temperature dependent mass densities of H_2O and ^2H_2O were derived from spline interpolation of tabulated density data[11]. Lipid dispersions were transferred to 3.2 mL ultra-clear centrifuge tubes which were loaded into a Beckman TLS-55 centrifuge rotor and spun at 50,000xg for one hour in a temperature controlled Beckman TLX-100 centrifuge. A series of H_2O/^2H_2O ratios was prepared and lipid densities were judged from the crossover point of a floating pellet to a pellet forming at the bottom of the tube.

Rhodopsin M_I/M_{II} ratio—Proteoliposomes were diluted to a rhodopsin concentration of 0.2 0.25 mg/mL in pH 7.0 PIPES-buffered saline buffer and equilibrated at 37°C in a thermally regulated sample holder. The equilibrium constant K_{eq}=[M_{II}]/[M_I] was determined from rapidly acquired UV-vis spectra of the M_I/M_{II} equilibrium after bleaching rhodopsin to 15 20% by a 520-nm flash. Individual M_I and M_{II} spectra were deconvolved from spectra of their equilibrium mixture as described previously[8]. The concentration of the photointermediates M_I and M_{II} were determined using extinction coefficients of 44,000 cm^{-1} and 38,000 cm^{-1} at their absorbance maxima of 478 nm and 365 nm, respectively.

Results

PE phase diagram—The phase state of the PE/water samples was determined by ^{31}P NMR as a function of temperature over the range of 5–50°C (Fig. 2). The phase diagram shows that at temperatures above 25°C, $18:0_{d35}$-$22:6_{n-3}$PE forms an H_{II} phase at all water concentrations. The phase diagram of $18:0_{d35}$-$22:5_{n-6}$PE and $18:1_{n-9}$-$18:1_{n-9}$PE[12] are very similar to the phase diagram shown in Fig. 3. Therefore, the properties of PE monolayers in the H_{II} phase were studied at a temperature of 30°C.

Chain order parameters—The order parameters of the saturated stearoyl hydrocarbon chains at position *sn-1* of the polyunsaturated $18:0_{d35}$-$22:6_{n-3}$PE and $18:0_{d35}$-$22:5_{n-6}$PE were determined by measurement of the ^2H-NMR quadrupolar splittings of methylene and methyl groups. The so-called de-Paked ^2H spectra[13], equivalent to spectra acquired on an oriented H_{II} phase with the long axis of inverse hexagonal H_{II} micelles parallel to the main magnetic field, B_0, are shown in Fig. 4. The corresponding order parameters were calculated according to the equation[14]

$$\Delta\nu_q = \frac{3}{2}\frac{e^2qQ}{h}S_{C^2H} \quad (1)$$

where $\Delta\nu_q$ is the measured quadrupolar splitting, $3/2(e^2qQ/h)$=250 kHz for a C-^{2}H bond and S_{C^2H} is the bond order parameter. Lipids in an inverse hexagonal phase reorient about an axis radial to the H_{II} micelles at correlation times on the order of nanoseconds and reorient by diffusion about the circular micelles at correlation times in the microsecond range. It can be shown that the latter, slower motion reduces lipid order parameters by a factor of ½ compared to a fluid lamellar lipid phase[15]. The corresponding order parameter profile of the *sn-1* hydrocarbon chains is shown in Fig. 5.

The lipid order of stearic acid in an H_{II} phase decreases steadily from methylene group C_2 towards the terminal methyl group. This is in contrast to order in lamellar lipid phases that has an order parameter plateau for chain segments $C_{2–8}$ and declining order for $C_{9–18}$. The difference reflects the different lipid geometry in fluid lamellar and H_{II} phases. While lipids in a lamellar phase occupy the volume of a cylinder, in the H_{II} phase they occupy the volume of a cone with small area at the headgroup and a larger area at the hydrocarbon chains (see Fig. 6). The larger area at the level of chains translates into larger amplitudes of orientational fluctuations of methylene segments which yields lower chain order parameters, in particular for methylene segments $C_{9–18}$. Lower order near the carboxyl group of stearic acid could be related to systematic changes of chain tilt upon diffusion about hexagonal phase cylinders as discussed by Hamm and Kozlov[17].

H_{II} phase dimensions—The repeat spacing of the H_{II} phases of all three PEs was determined by x-ray diffraction at a temperature of 30°C. The geometry of an H_{II} phase is shown in Fig. 6. The lipids form inverted tubular micelles with a water-filled core. The tubular micelles are arranged in a hexagonal lattice with the repeat spacing d_{hex} as shown in Fig. 6.

The repeat spacing d_{hex} as a function of osmotic pressure, π, for the PEs is shown in Fig. 7.

Monolayer elastic properties—With increasing osmotic pressure, the volume of the water core and the radius of curvature of the inverse micelles decrease which results in decreased repeat spacings d_{hex}. The change of the radius of curvature of lipid monolayers in the inverse micelles under osmotic stress yields the energy of monolayer bending. The calculation requires knowledge of the number of water molecules per PE molecule in the

water-filled core. Water content was determined by comparison of integral intensity of the ^{1}H resonance of water to integral intensity of lipid resonances in the ^{1}H-MAS NMR spectra of H_{II} phases that were equilibrated against PEG20,000 water solutions. The water content as a function of PEG20,000 concentration is shown in Fig. 8.

The energy of bending of a lipid monolayer can be approximated by the equation[18, 19]

$$F=\frac{1}{2}K_{cp}A_p\left(\frac{1}{R_p}-\frac{1}{R_{0p}}\right)^2, \quad (2)$$

where K_{cp} is the elastic bending modulus, A_p, the area per lipid molecule at the radius R_p, and R_{0p} the spontaneous radius of curvature. Following procedures reported by Rand, Gruner, and Parsegian[7, 20], we relate the elastic energy given by eq. 2 tothe osmotic work done by applying osmotic stress **π**:

$$\pi R_p^2=2K_{cp}\left(\frac{1}{R_p}-\frac{1}{R_{0p}}\right). \quad (3)$$

The density measurements at 30°C yield specific volumes per molecule of 18:0$_{d35}$-22:6$_{n-3}$PE and 18:1$_{n-9}$-18:1$_{n-9}$PE of 1,282 A and 1,218 Å^3, respectively. The specific volume of 18:0$_{d35}$-22:5$_{n-6}$PE is 1,294 Å^3, as calculated from the specific volume of 18:0$_{d35}$-22:6$_{n-3}$PE with a correction for the number of –CH$_2$ and =CH groups per *sn-2* chain with the specific volumes of 28.14 Å^3 and 22.31 Å^3, respectively[21]. The analysis yielded the elastic parameters of lipid monolayers in the H_{II} phase as reported in Tab. 2.

M_I/M_{II} equilibrium of rhodopsin—Dark adapted bovine rhodopsin was reconstituted into 16:0-18:1$_{n-9}$PC bilayers containing 0–75 mol% of 18:0-22:6$_{n-3}$PE, 18:0-22:5$_{n-6}$PE, or 18:1$_{n-9}$-18:1$_{n-9}$PE, respectively. Up to PE concentrations of 75 mol%, the reconstituted proteoliposomes remained in a lamellar phase. With increasing PE concentration, the M_I/M_{II} equilibrium shifted towards M_{II} as reported earlier[3,4]. Experimental results shown in Fig. 10 are extrapolated to 100% PE in the membrane.

Let's assume that the difference in free energy between the M_I and M_{II} photointermediates of rhodopsin in lipid bilayers is due to differences in curvature elastic stress of lipid monolayers. Following the flexible surface model of Brown[3], it can be shown that the change in free energy of rhodopsin is

$$\Delta G=-\mathrm{kT}\ln K_{eq}, \quad (4)$$

and

$$\Delta(\Delta G)=\frac{n_L}{kT}\left(\frac{K_{cp}^{l2}\times A_p^{l2}}{R_{0p}^{l2}}-\frac{K_{cp}^{l1}\times A_p^{l1}}{R_{0p}^{l1}}\right)\times\left(\frac{1}{R_{MII}}-\frac{1}{R_{MI}}\right), \quad (5)$$

where k is the Boltzmann constant, T the absolute temperature, $K_{eq}=[M_{II}]/[M_I]$ the ratio of concentrations of photointermediates M_{II} and M_I, n_L the number of lipids per protein molecule, K_{cp}^{l1} and K_{cp}^{l2} are the bending elastic coefficients of lipids 1 and 2, A_p^{l1} and A_p^{l2} are the areas at the pivotal plane of lipids 1 and 2, R_{0p}^{l1} and R_{0p}^{l2} are the radii of spontaneous

monolayer curvature at the pivotal plane for lipids 1 and 2, and R_{MI} and R_{MII} are the radii of lipid monolayer curvature near the photointermediates M_I and M_{II}, respectively. For derivation of equ. 5 it was assumed that the protein-induced monolayer curvatures R_{MI} and R_{MII} are constant throughout the membrane and independent of lipid composition[4]. The value of the factor $(1/R_{MII}\text{-}1/R_{MI})$ was adjusted to fit the span of experimentally measured values of $\Delta(\Delta G)$ (see Fig. 10) which yielded $(1/R_{MII}\text{-}1/R_{MI})=2.36\text{x}10^{-4}$ AÅ^{-1}. The spontaneous monolayer curvature of 16:0-18:1$_{n\text{-}9}$PC was assumed to be ∞. In Fig. 10, the $\Delta(\Delta G)$ energies relative to 16:0-18:1$_{n\text{-}9}$PC bilayers for a series of lipids are shown. Results for lipids that are not reported in this paper were taken from our previous publication[4].

Discussion

It was determined that the polyunsaturated lipids 18:0-22:6$_{n\text{-}3}$PE and 18:0-22:5$_{n\text{-}6}$PE and the model lipid 18:1$_{n\text{-}9}$-18:1$_{n\text{-}9}$PE form lipid monolayers in a H_{II} phase with very small spontaneous radii of curvature. While the model lipid 18:1$_{n\text{-}9}$-18:1$_{n\text{-}9}$PE (DOPE) is uncommon, PE with the polyunsaturated docosahexaenoic acid (22:6$_{n\text{-}3}$, DHA) is found at high concentrations in the brain, retina, and sperm of mammals[2]. It was observed that high DHA concentrations are critical for proper brain development and function[22]. In animal and human infant studies it was shown that deficiency in ω-3 fatty acids is associated with visual and cognitive deficits[23, 24]. In cases of an insufficient supply of ω-3 fatty acids, DHA is replaced by docosapentaenoic acid (22:5$_{n\text{-}6}$, DPA$_{n\text{-}6}$), an ω-6 fatty acid with one less double bond at the methyl terminal end of the chain. Such replacement may not be lethal, but has been related to some loss in function[2, 25, 26].

Our results show convincingly that membranes with high content of polyunsaturated PEs have monolayers that are under severe negative curvature elastic stress. The series of lipids in Fig. 9 shows that such increasing curvature stress favors formation of the photointermediate M_{II} that is capable of activating the G protein transducin.

Recent observations on the mechanism of photoactivation of rhodopsin provide a plausible cause for the shift of the M_I/M_{II} equilibrium towards M_{II} under negative curvature elastic stress. The transition from M_I to M_{II} is associated with an outward tilt of transmembrane helix VI of rhodopsin[27, 28]. The photointermediate M_{II} tends to be more hourglass-shaped as shown in Fig. 11. This induces negative curvature in lipid monolayers near the protein and releases curvature stress in the M_{II}-lipid domain and, therefore, favours formation of the photointermediate M_{II}. Since there is a steady increase in the amount of M_{II} with increasing negative curvature elastic stress (see Fig. 10), curvature stress appears to be the most important mechanism that shifts the M_I-M_{II} equilibrium.

The replacement of the ω-3 polyunsaturated 18:0-22:6$_{n\text{-}3}$PE by the ω-6 polyunsaturated 18:0-22:5$_{n\text{-}6}$PE with just one fewer double bond results experimentally in a somewhat lower formation of M_{II}, similar to values observed for the model lipid 18:1$_{n\text{-}9}$-18:1$_{n\text{-}9}$PE. The differences in calculated curvature elastic stress for monolayers of all three lipids are not statistically significant. According to predictions from measurements on H_{II} phases, all three lipids form monolayers that are under high curvature elastic stress in membranes. Therefore one could argue that 18:0-22:5$_{n\text{-}6}$PE that is formed under conditions of dietary deficiencies of ω-3 fatty acids is the next best substitute for 18:0-22:6$_{n\text{-}3}$PE, although, experimentally it seems to be somewhat inferior.

Regarding the quantitative comparison between monolayer elastic properties in a H_{II} phase probed by application of osmotic stress and shifts in rhodopsin function a word of caution is advisable. The coefficients of curvature elasticity have been fitted to data obtained over a limited range of curvatures, most of them rather small. When extrapolating results to

curvature near rhodopsin, a wider range of curvatures is probed, from smaller radii near the protein to flat monolayers further away from the protein where R_p approaches infinity. The latter case is well outside the range for which elastic properties have been determined. Furthermore, the assumptions used to derive eq. 5 are rather crude (see Soubias et al.[4]) leaving room for improvement. A more detailed analysis of decay of perturbations in the lipid matrix with increasing distance from the protein that also takes into consideration that lipids have a tilt degree of freedom, not just bending, is required[17]. Furthermore, the lipid-protein interface is inhomogeneous in terms of lipid-protein interaction about the protein circumference[29–31].

It was shown that the elastic response of the protein to the frustrated spontaneous curvature of the component lipid monolayer leaflets is equivalent to the response of the protein to a membrane lateral pressure profile[32]. The curvature elastic data for the lipids $18{:}1_{n\text{-}9}$-$18{:}1_{n\text{-}9}$PC and $18{:}1_{n\text{-}9}$-$18{:}1_{n\text{-}9}$PE were used for evaluation of possible differences in rhodopsin geometry between M_I and M_{II}[32].

Recently, a series of crystal structures of rhodopsin-like GPCR have been published, among them the important dopaminergic[33] and adrenergic receptors[34–36]. The data show convincingly that class A GPCR have a lot of common functional motives, although similarities in amino acid sequences are rather limited. Therefore we propose that bovine rhodopsin may serve as convenient representative of class A GPCR to study the influence of lipid matrix properties on function. The ligand 11-cis-retinal is a powerful inverse agonist that provides great stability to dark adapted rhodopsin[37]. However, all-trans-retinal that is formed by photoactivation seems to be a weak agonist which generates variable amounts of M_{II} depending on environmental conditions. It has been widely discussed that GPCR activation is under heavy influence of allosteric modulators[38]. The data on the influence of the lipid matrix on rhodopsin function suggest that the properties of the lipid matrix are, perhaps, the most important allosteric modulator of GPCR function.

There is an important difference between rhodopsin and other GPCR. While rhodopsin has no constitutive activity without photoactivation, most other GPCR have substantial constitutive activity in the absence of a ligand[39]. Such constitutive activity is likely to be most dependent on composition of the lipid matrix.

Conclusions

Negative curvature elastic stress in membranes containing high concentrations of polyunsaturated PEs is very high. Release of even a small fraction of this stress from the layer of lipids surrounding the receptor is sufficient to shift the M_I/M_{II} equilibrium towards M_{II}, the state that activates G protein. Furthermore, polyunsaturated bilayers have a hydrophobic thickness of about 27 Å which has been determined to match the length of the hydrophobic transmembrane helices of rhodopsin[40]. The data show that polyunsaturated lipids are important for class A GPCR activation, and we speculate that the rhodopsin model is particularly relevant for constitutive activity of GPCR and activation by weak agonists.

Acknowledgments

This work was supported by the Intramural Research Program of the National Institute on Alcohol Abuse and Alcoholism, National Institutes of Health.

Notes and references

1. Boesze-Battaglia K, Albert AD. Exp Eye Res. 1992; 54:821–823. [PubMed: 1623969]

2. Salem, N.; Spiller, GA.; Scala, A. New Protective Roles for Selected Nutrients. Alan R. Liss, Inc; New York: 1989. p. 109-228.
3. Botelho AV, Gibson NJ, Thurmond RL, Wang Y, Brown MF. Biochemistry. 2002; 41:6354–6368. [PubMed: 12009897]
4. Soubias O, Teague WE Jr, Hines KG, Mitchell DC, Gawrisch K. Biophys J. 2010; 98:817–824. [PubMed: 20682259]
5. Parsegian VA, Rand RP, Fuller NL, Rau DC. Methods Enzymol. 1986; 127:400–416. [PubMed: 3736427]
6. Rand RP, Parsegian VA. Current Topics in Membranes. 1997; 44:167–189.
7. Gruner SM, Parsegian VA, Rand RP. Faraday Discuss Chem Soc. 1986; 81:29–37. [PubMed: 3582619]
8. Straume M, Mitchell DC, Miller JL, Litman BJ. Biochemistry. 1990; 29:9135–9142. [PubMed: 2271583]
9. Litman BJ, Lester P. Methods Enzymol. 1982; 81:150–153. [PubMed: 7098858]
10. Wald G, Brown PK. J Gen Physiol. 1953; 37:189–200. [PubMed: 13109155]
11. Lide, DR. Handbook of Chemistry and Physics. CRC Press; Boca Raton: 2004.
12. Gawrisch K, Parsegian VA, Hajduk DA, Tate MW, Graner SM, Fuller NL, Rand RP. Biochemistry. 1992; 31:2856–2864. [PubMed: 1550812]
13. Sternin E, Bloom M, MacKay AL. J Magn Reson. 1983; 55:274–282.
14. Davis JH, Jeffrey KR, Bloom M, Valic MI, Higgs TP. Chem Phys Lett. 1976; 42:390–394.
15. Seelig J. Biochim Biophys Acta. 1978; 515:105–140. [PubMed: 356883]
16. Holte LL, Peter SA, Sinnwell TM, Gawrisch K. Biophys J. 1995; 68:2396–2403. [PubMed: 7647244]
17. Hamm M, Kozlov MM. Europ Phys J B. 1998; 6:519–528.
18. Helfrich W. Z Naturforsch. 1973; 28c:693–703.
19. Kirk GL, Gruner SM, Stein DL. Biochemistry. 1984; 23:1093–1102.
20. Rand RP, Fuller NL, Gruner SM, Parsegian VA. Biochemistry. 1990; 29:76–87. [PubMed: 2322550]
21. Koenig BW, Gawrisch K. Biochim Biophys Acta. 2005; 1715:65–70. [PubMed: 16109383]
22. Salem N, Litman B, Kim HY, Gawrisch K. Lipids. 2001; 36:945–959. [PubMed: 11724467]
23. Neuringer M, Connor WE, Lin DS, Barstad L, Luck S. Proc Natl Acad Sci USA. 1986; 83:4021–4025. [PubMed: 3459166]
24. O'Connor DL, Hall R, Adamkin D, Auestad N, Castillo M, Connor WE, Connor SL, Fitzgerald K, Groh-Wargo S, Hartmann EE, Jacobs J, Janowsky J, Lucas A, Margeson D, Mena P, Neuringer M, Nesin M, Singer L, Stephenson T, Szabo J, Zemon V, Ross S. Preterm Lipid. Pediatrics. 2001; 108:359–371. [PubMed: 11483801]
25. Salem, N., Jr; Kim, HY.; Yergey, JA. Health Effects of Polyunsaturated fatty Acids in Seafoods. Simopoulos, AP.; Kifer, RR.; Martin, RE., editors. Academic Press; New York: 1986. p. 319-351.
26. Moriguchi T, Greiner RS, Salem N. J Neurochem. 2000; 75:2563–2573. [PubMed: 11080210]
27. Altenbach C, Kusnetzow AK, Ernst OP, Hofmann KP, Hubbell WL. Proc Natl Acad Sci USA. 2008; 105:7439–7444. [PubMed: 18490656]
28. Choe HW, Kim YJ, Park JH, Morizumi T, Pai EF, Krauss N, Hofmann KP, Scheerer P, Ernst OP. Nature. 2011; 471:651–U137. [PubMed: 21389988]
29. Soubias O, Teague WE, Gawrisch K. J Biol Chem. 2006; 281:33233–33241. [PubMed: 16959786]
30. Periole X, Huber T, Marrink SJ, Sakmar TP. J Am Chem Soc. 2007; 129:10126–10132. [PubMed: 17658882]
31. Mondal S, Khelashvili G, Shan J, Andersen OS, Weinstein H. Biophys J. 2011; 101:2092–2101. [PubMed: 22067146]
32. Marsh D. Biophys J. 2007; 93:3884–3899. [PubMed: 17704167]
33. Chien EYT, Liu W, Zhao Q, Katritch V, Han GW, Hanson MA, Shi L, Newman AH, Javitch JA, Cherezov V, Stevens RC. Science. 2010; 330:1091–1095. [PubMed: 21097933]

34. Rosenbaum DM, Zhang C, Lyons JA, Holl R, Aragao D, Arlow DH, Rasmussen SGF, Choi HJ, DeVree BT, Sunahara RK, Chae PS, Gellman SH, Dror RO, Shaw DE, Weis WI, Caffrey M, Gmeiner P, Kobilka BK. Nature. 2011; 469:236–240. [PubMed: 21228876]

35. Rasmussen SGF, Choi HJ, Fung JJ, Pardon E, Casarosa P, Chae PS, DeVree BT, Rosenbaum DM, Thian FS, Kobilka TS, Schnapp A, Konetzki I, Sunahara RK, Gellman SH, Pautsch A, Steyaert J, Weis WI, Kobilka BK. Nature. 2011; 469:175–180. [PubMed: 21228869]

36. Warne T, Moukhametzianov R, Baker JG, Nehme R, Edwards PC, Leslie AGW, Schertler GFX, Tate CG. Nature. 2011; 469:241–244. [PubMed: 21228877]

37. Bennett MP, Mitchell DC. Biophys J. 2008; 95:1206–1216. [PubMed: 18424497]

38. Melancon BJ, Hopkins CR, Wood MR, Emmitte KA, Niswender CM, Christopoulos A, Conn PJ, Lindsley CW. J Med Chem. 2012; 55:1445–1464. [PubMed: 22148748]

39. Seifert R, Wenzel-Seifert K. Naunyn-Schmiedebergs Arch Pharmacol. 2002; 366:381–416. [PubMed: 12382069]

40. Soubias O, Gawrisch K. Biochim Biophys Acta. 2012; 1818:234–240. [PubMed: 21924236]

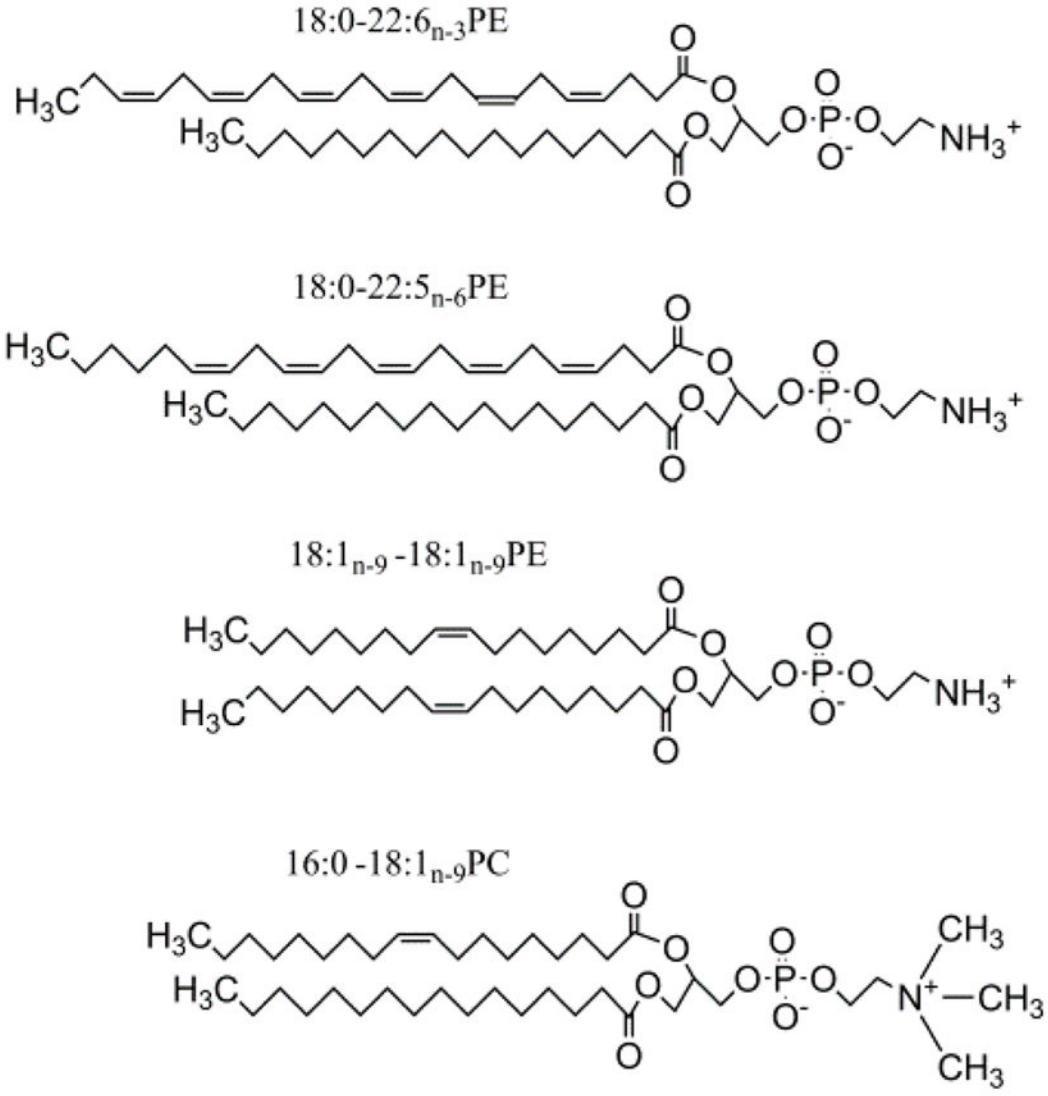

Fig. 1.

The lipids 1-perdeuterio-stearyl-2-docosahexaenoyl-*sn*-glycero-3-phosphoethanolamine ($18:0_{d35}$-$22:6_{n-3}$PE), 1-perdeuterio-stearyl-2-docosapentaenoyl-*sn*-glycero-3-phosphoethanolamine ($18:0_{d35}$-$22:5_{n-6}$PE), 1,2-dioleoyl-*sn*-glycero-3-phosphoethanolamine ($18:1_{n-9}$-$18:1_{n-9}$PE), and 1-palmitoyl-2-oleoyl-*sn*-glycero-3-phosphocholine (16:0-$18:1_{n-9}$PC).

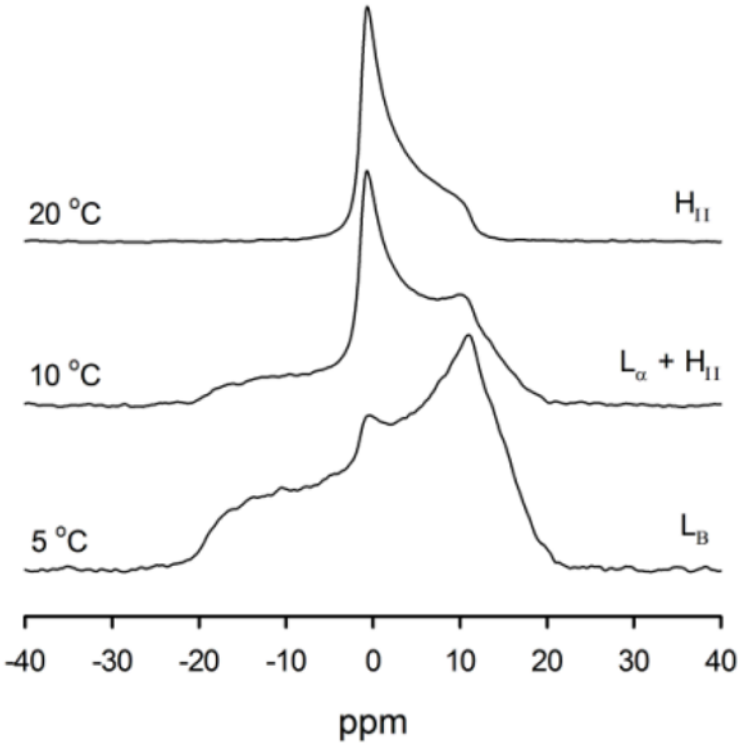

Fig. 2.

^{31}P NMR spectra of a 18:0$_{d35}$-22:6$_{n-3}$PE sample containing 6.9 water molecules per lipid. With increasing temperature, the sample converted from a crystalline L_β-phase to coexisting L_α- and H_{II} phases and finally to a H_{II} phase.

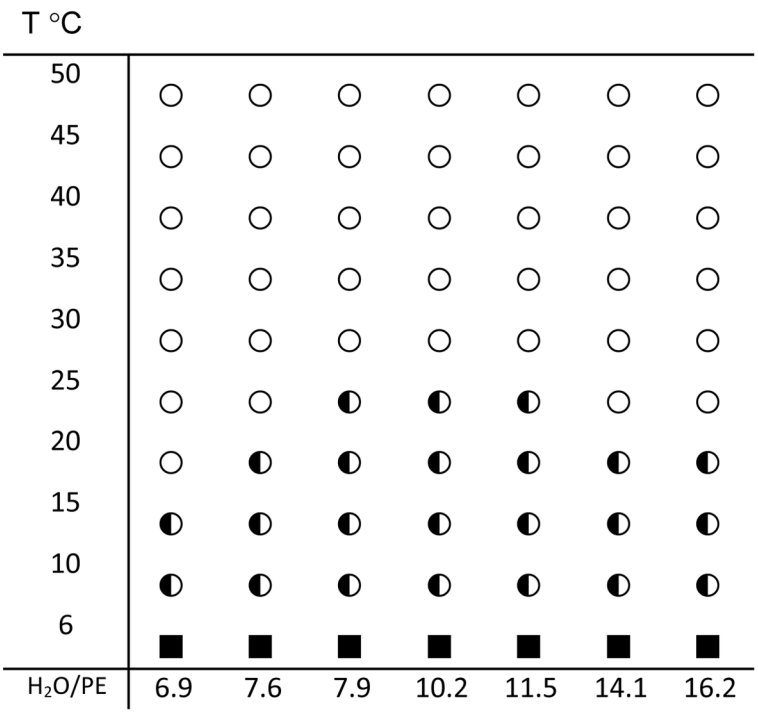

Fig. 3.

Phase diagram of $18{:}0_{d35}$-$22{:}6_{n\text{-}3}$PE as a function of water content and temperature. ○ - inverse hexagonal phase, $H_{II;}$ ◐- mixture of hexagonal, H_{II}, and liquid-crystalline lamellar, L_{α}, phases; ■ - crystalline lamellar, L_{β}, phase

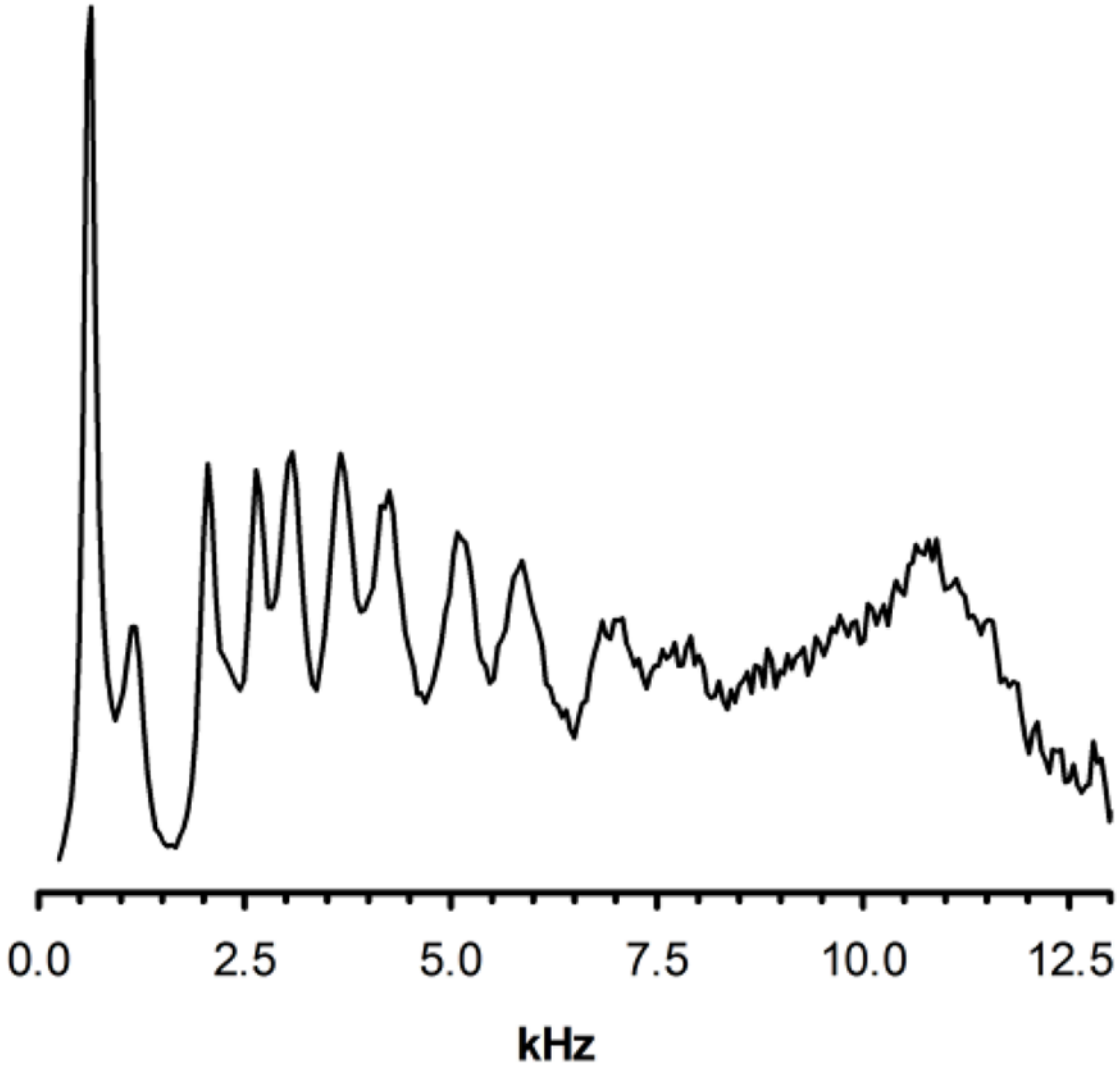

Fig. 4.

De-Paked ^{2}H NMR spectrum of 18:0$_{d35}$-22:6$_{n-3}$PE acquired at a temperature of 30°C. Only the right half of the symmetrical spectrum is shown. The resolved peaks correspond to the quadrupolar splittingsof the aliphatic groups of stearic acid beginning with the terminal methyl group on the left and ending with methylene group, C_2, at the carboxyl end.

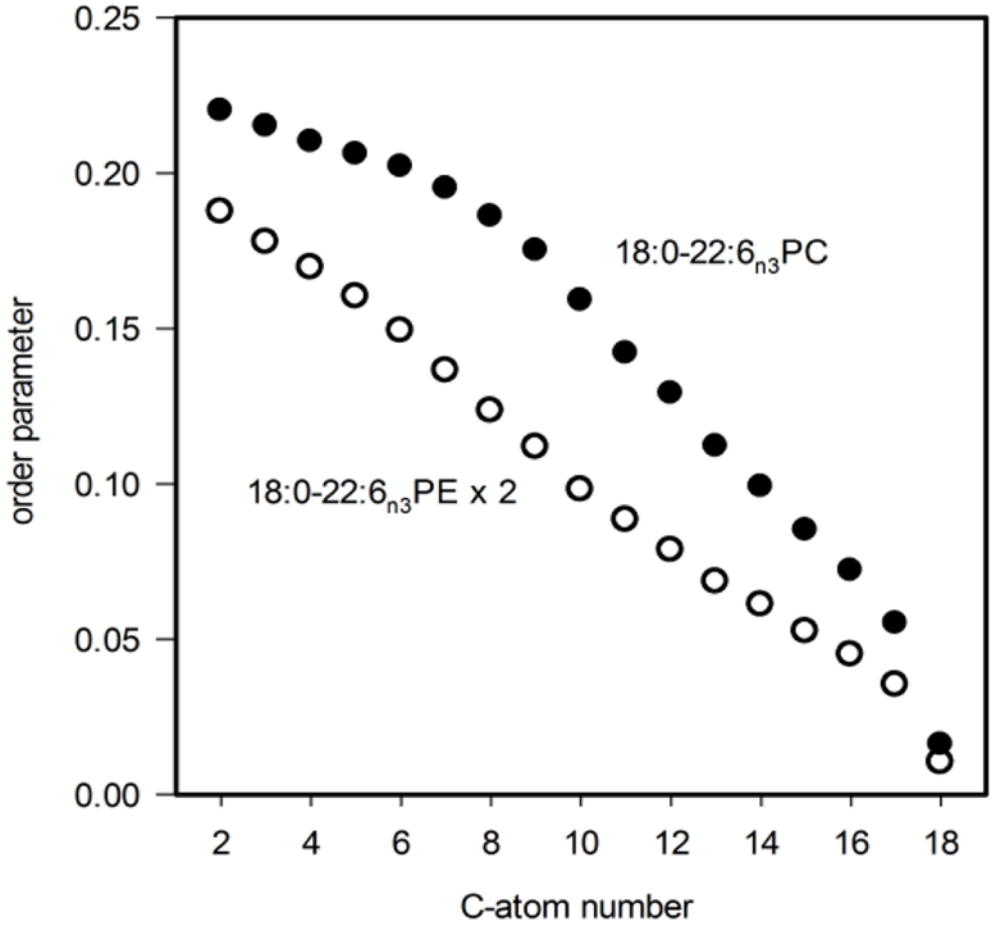

Fig. 5.

Order parameter profile of the *sn-1* chain in $18{:}0_{d35}$-$22{:}6_{n-3}$PE (open circles) in comparison to the order parameter profiles of $18{:}0_{d35}$-$22{:}6_{n-3}$PC (filled circles)[16]. The order parameters of $18{:}0_{d35}$-$22{:}6_{n-3}$PE are multiplied by a factor of two to eliminate order reduction from diffusion about the tubular H_{II} phase micelles.

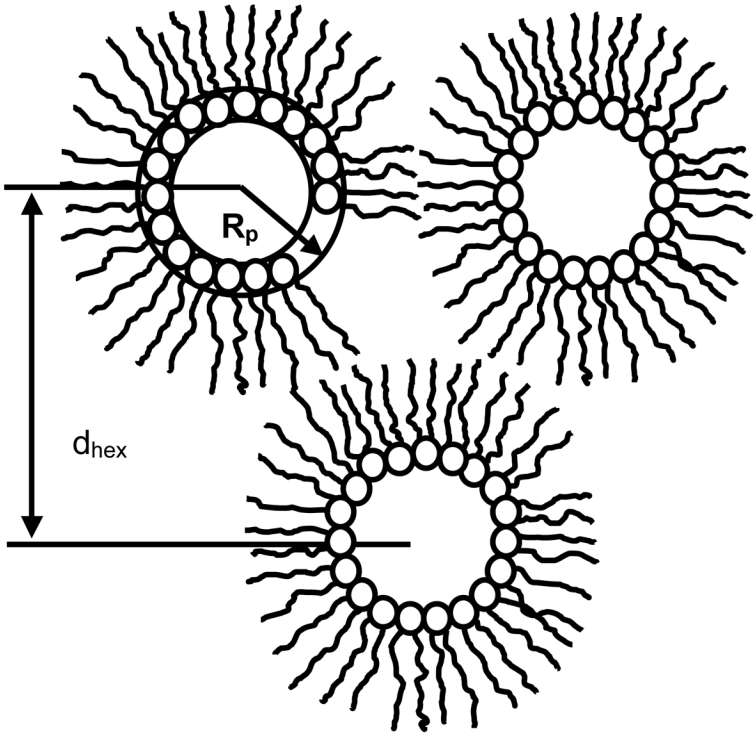

Fig. 6.

Arrangement of cylindrical micelles in an inverse hexagonal, H_{II} phase. The core of the micelles is filled with water. The repeat spacing d_{hex} is measured by x-ray diffraction. Dehydration of H_{II} micelles by application of controlled osmotic stressfrom PEG/water solutions reduces the water volume and changes the radius of micelles, R_p, measured at the pivotal plane.

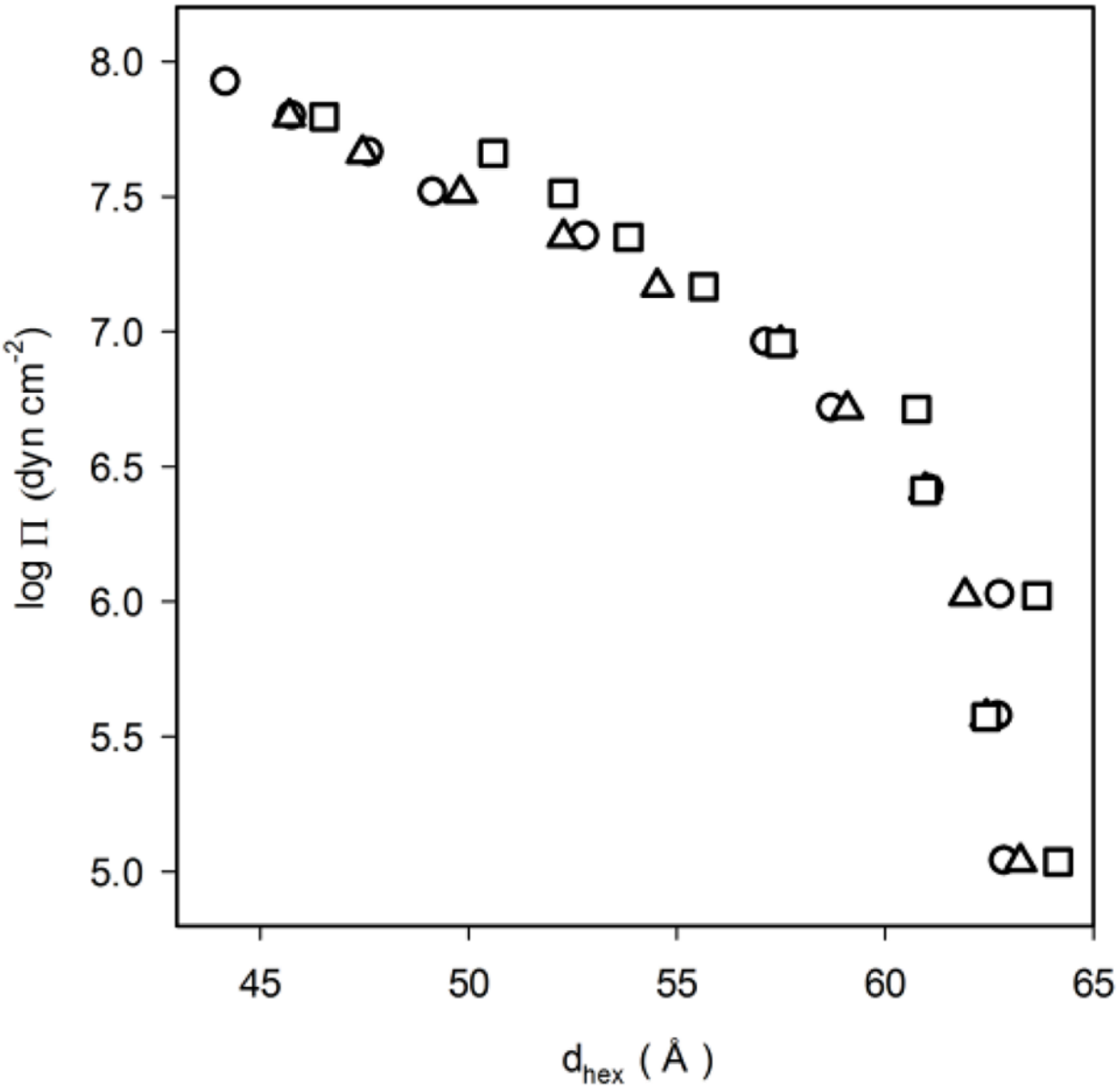

Fig. 7.

Repeat spacings d_{hex} for $18{:}0_{d35}$-$22{:}6_{n-3}$PE (squares), $18{:}0_{d35}$-$22{:}5_{n-6}$ PE (triangles), and $18{:}1_{n-9}$-$18{:}1_{n-9}$PE (circles) as a function of osmotic pressure of PEG20,000.

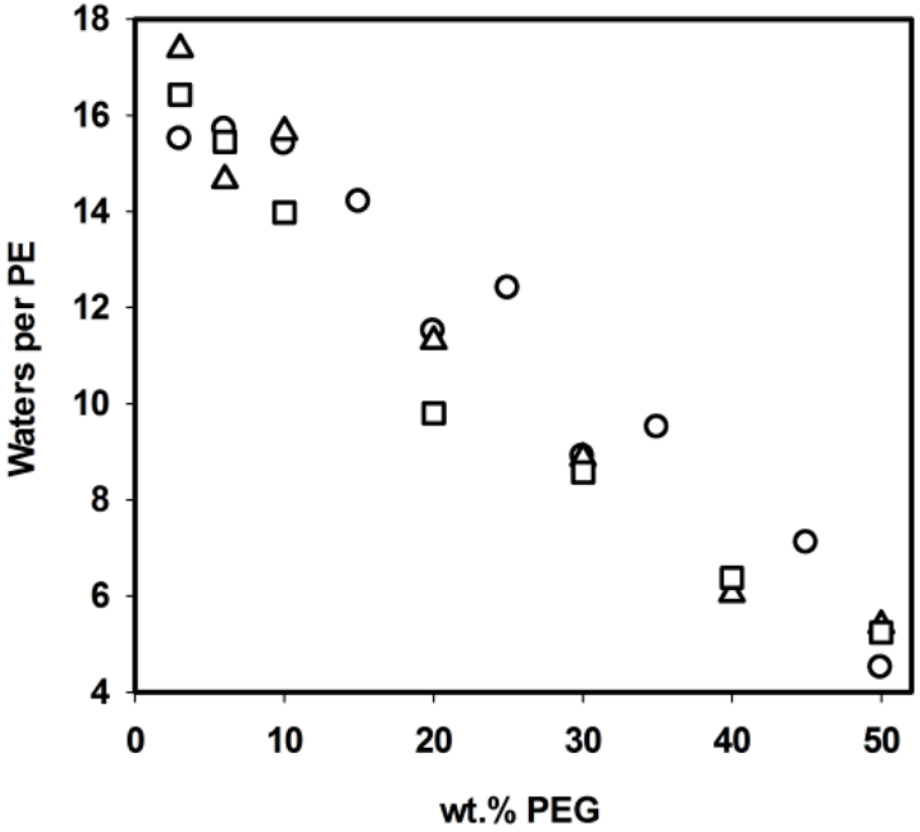

Fig. 8.

Number of water molecules per PE in H_{II} phases of $18{:}0_{d35}$-$22{:}6_{n\text{-}3}$PE (squares), $18{:}0_{d35}$-$22{:}5_{n\text{-}6}$PE (triangles), and $18{:}1_{n\text{-}9}$-$18{:}1_{n\text{-}9}$PE (circles) as a function of PEG20,000 concentration in wt.%.

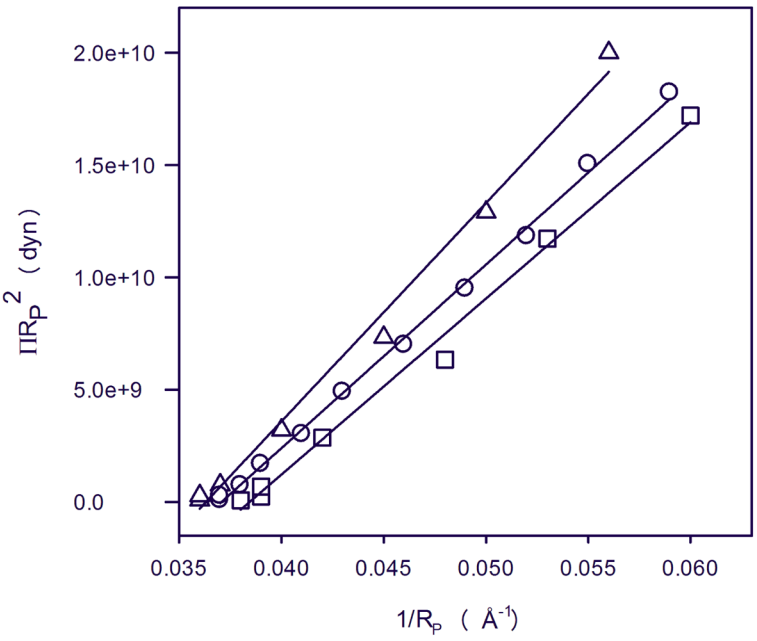

Fig. 9.

Plot relating the osmotic work to dehydrate the hexagonal phase to the change in monolayer curvature, $1/R_p$, for $18{:}0_{d35}$-$22{:}6_{n-3}$PE (squares), $18{:}0_{d35}$-$22{:}5_{n-6}$PE (triangles), and $18{:}1_{n-9}$-$18{:}1_{n-9}$PE (circles). The fit to the data points yields the bending elastic modulus, K_{cp}, and the spontaneous radius of monolayer curvature, R_{0p}.

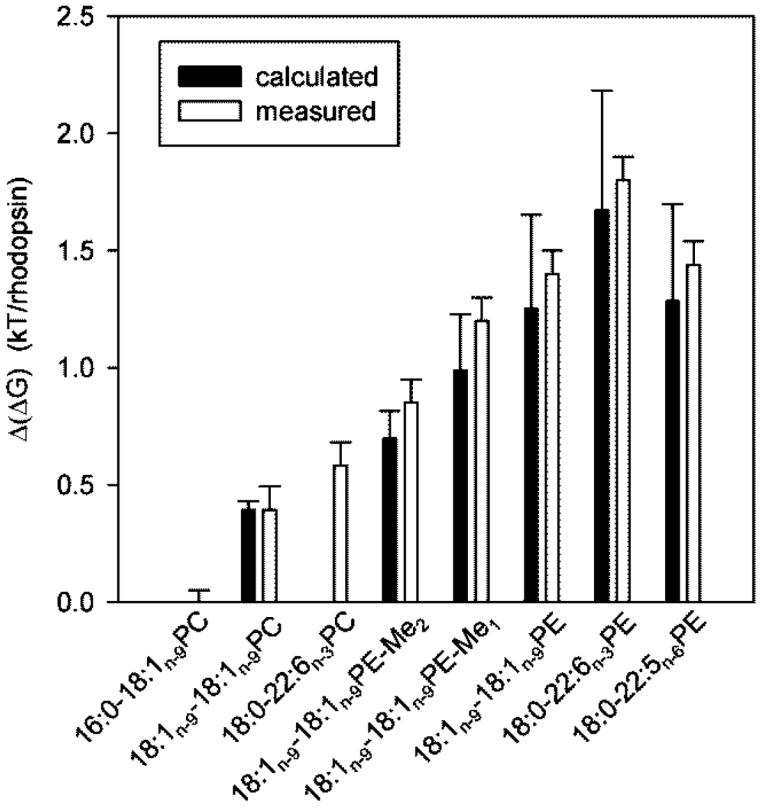

Fig. 10.

Measured and calculated energetic differences Δ(ΔG) between photointermediates M_I and M_{II} in membranes composed of lipids with increasing negative curvature elastic stress (see eq. 4,5). Experiments were conducted at a rhodopsin/lipid ratio of 1/250. Data are reported relative to 16:0-18:1_{n-9}PC, a lipid with negligible curvature elastic stress. Experimental data for PEs could be obtained up to a concentration of 75 mol% PE in membranes only. Results shown in this figure are linearly extrapolated to 100% PE.

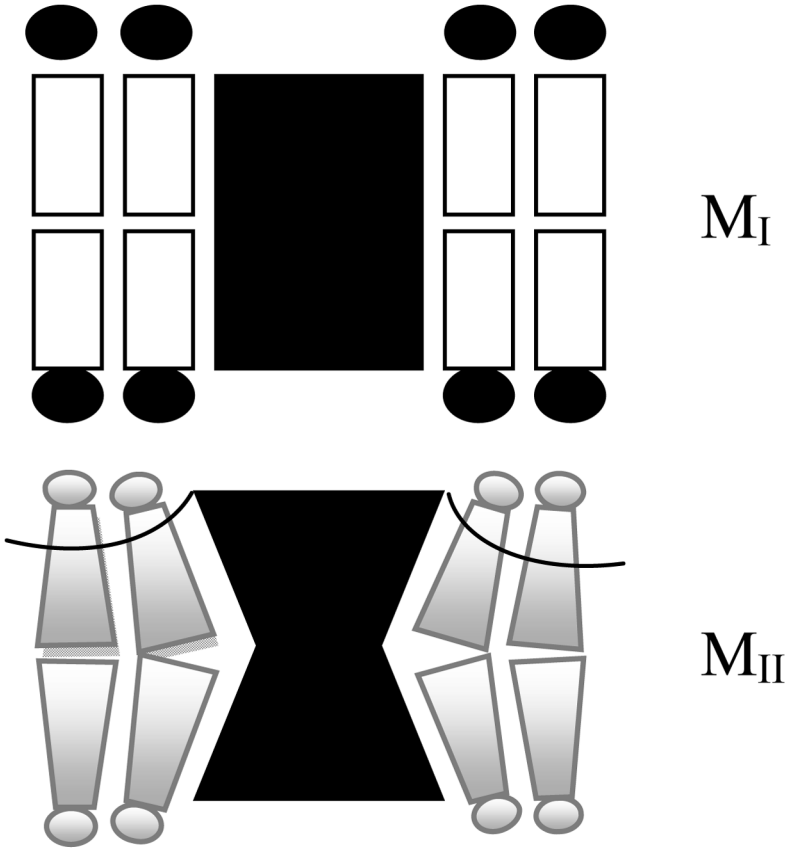

Fig. 11.

Cartoon highlighting the structural differences between the rhodopsin photointermediates M_I and M_{II}. Structural data on M_I and M_{II} suggest that M_{II} tends to be more hourglass-shaped. This generates negative curvature in lipid monolayers near the protein. Please note that structural differences are exaggerated for clarity.

Tab. 2

Elastic Parameters of Lipid Monolayers

Lipid	A_p (Å^2)[a]	K_{cp} (kT/molec.) [b]	R_{0p} (Å)[c]
18:0-22:6$_{n-3}$PE	65.5	11.7	27.5
18:0-22:5$_{n-6}$PE	58.9	9.3	26.0
18:1$_{n-9}$-18:1$_{n-9}$PE	61.2	9.9	26.9

[a] ±2 Å^2;

[b] ±1 kT/molec.;

[c] ±2 Å